Sliding Geometries in Deformable Image Registration

Danielle F. Pace[1], Marc Niethammer[2], and Stephen R. Aylward[1]

[1] Kitware Inc., Clifton Park NY and Carrboro NC, USA
danielle.pace@kitware.com, stephen.aylward@kitware.com
[2] The University of North Carolina at Chapel Hill, Chapel Hill NC, USA
mn@cs.unc.edu

Abstract. Regularization is used in deformable image registration to encourage plausible displacement fields, and significantly impacts the derived correspondences. Sliding motion, such as that between the lungs and chest wall and between the abdominal organs, complicates registration because many regularizations are global smoothness constraints that produce errors at object boundaries. We present locally adaptive regularizations that handle sliding objects with locally planar and tubular geometries. These regularizations allow discontinuities to develop in the displacement field at sliding interfaces and increase the independence with which regions surrounding distinct geometric structures can behave. Validation is performed by registering inhale and exhale abdominal computed tomography (CT) images and artificial images of a sliding tube. The sliding registration methods produce more realistic correspondences that may better reflect the underlying physical motion, while performing as well as the diffusive regularization with respect to image match.

1 Introduction

Within many clinical workflows, the goal of deformable image registration is to (1) quantify treatment effectiveness by measuring change within longitudinal datasets or across subjects, (2) map surgical plans from preoperative images onto intraoperative images for guidance, or (3) align atlases with patient images to map auxilliary information from the atlas, such as expected functional site localizations, into the patient. To successfully accomplish thse tasks, it is critical to establish accurate correspondence between the images. However, establishing correspondence using a deformable image registration method that optimizes image match alone is ill-posed, i.e. there exist many displacement fields that produce the same transformed moving image [5].

To obtain sensible correspondences using deformable image registration, a regularization term is typically introduced to encourage a smooth displacement field. The registration result is therefore a compromise between image similarity and spatial regularity, and the regularization forms a strong prior on the final transformation. This is true for any non-corner or point structure due to spatial ambiguity (the so-called aperture effect). Registration results are dependent on

relatively sparse features and regularization drives the estimation of otherwise unobservable deformations within homogeneous regions.

The focus of this paper is on accurately registering images that depict sliding motion between multiple structures. This includes the sliding of the abdominal organs and lungs due to respiration. Here, the assumption of a globally smooth displacement field is inappropriate, as globally smoothing regularizations, such as the diffusive regularization, cannot recover the motion discontinuities that arise at the interfaces between sliding structures. Locally adaptive regularizations [2, 9] vary spatially and can more accurately capture complex deformations.

Several regularizations aiming to handle sliding motion have been presented, but have typically been applied to the alignment of lung images. These include investigations of non-quadratic regularizers [4], a volume-preserving regularization that allows shear discontinuities at sliding interfaces [7], and regularizations based on anisotropic diffusion that use supplied organ segmentations [6, 8, 10]. We take this last approach here. Yin *et al.* [10] tailor their regularization towards the biomechanics of lung lobar fissures using spatially-varying isotropic smoothing. Schmidt *et al.* [8] implement sliding motion by smoothing the displacement components tangential to the sliding interface separately for a sliding object and within its background, using Neumann boundary conditions. We present a regularization that instead applies separate diffusion tensors to the normal and tangential displacements of the entire displacement field. This regularization natively handles multiple sliding organs and has been evaluated preliminarily using synthetic and phantom lung images [6].

The sliding regularizations based on anisotropic diffusion described above, including our own work [6], solely handle displacement field discontinuities at roughly planar interfaces between two sliding organs. By also adding notions of tubular and point-like structures, we present a regularization that handles sliding motion of planes and tubes and that smooths displacement fields according to local structure classifications. We refer to registration methods including this regularization as "geometry conditional registration methods".

We begin by outlining our sliding organ formulation, followed by a description of its extension to a geometry conditional deformable registration method that also considers tubular and point-like structures. Validation is conducted by performing intra-subject registrations between inhale and exhale computed tomography (CT) images and between artificial images depicting a sliding tube. These assessments demonstrate the increased plausibility of the resulting displacement field, which encapsulates the correspondence necessary to use registration in clinical tasks. Additionally, these results demonstrate the advantages of considering sliding motion throughout the abdomen.

2 Methods

2.1 Deformable non-parametric image registration

Given a target image T and a moving image M on the domain Ω, deformable non-parametric image registration aims to find a displacement field u that maps

the moving image onto the target such that $T(\mathbf{x}) \approx M(\mathbf{x}-u(\mathbf{x}))$ [5]. This is often performed by minimizing a cost function of the form $C(u) = D[T, M; u]+\alpha S(u)$. $D[T, M; u]$ is an image match distance measure between T and M under the current estimate of the displacement field u, and $S(u)$ is the regularization that penalizes unrealistic displacement fields.

2.2 Principles of sliding motion

Writing a regularization for use in registering images depicting sliding organs can be guided by decomposing the displacement field u into normal ($u^{\perp}$) and tangential ($u^{\parallel}$) displacements with respect to the organ boundary along which sliding is expected to occur. One can then consider the following principles [6, 8] close to sliding organ boundaries:

1. **Sliding motion:** Sliding causes the tangential displacements to be discontinuous along the normal direction(s).
2. **Intra-organ smoothness:** The displacements must be smooth along the tangential direction(s) to encourage smooth movement within individual structures.
3. **Inter-organ coupling:** Discontinuities in the normal displacements in the surface normal direction(s) are penalized to ensure organs do not pull apart (a valid assumption for many medical images).

2.3 Sliding organ registration

For sliding organ registration, we encapsulate these rules in a regularizer based on anisotropic diffusion [6]. Here, diffusion tensors specify the direction and strength of the intra-organ smoothness (IOS) and inter-organ coupling (IOC) constraints:

$$S_{sliding}(u) = \frac{1}{2} \sum_{l=x,y,z} \sum_{\mathbf{x}\in\Omega} \|D_{IOS}(\mathbf{x}) \nabla u_l(\mathbf{x}) + D_{IOC}(\mathbf{x}) \nabla u_l^{\perp}(\mathbf{x})\|^2 \qquad (1)$$

where ∇ is the gradient operator, $u_l(\mathbf{x})$ is the l^{th} scalar component of the displacement field, and $u_l^{\perp}(\mathbf{x})$ is the l^{th} scalar component of the normal component of the displacement field. If $n(\mathbf{x})$ is the normal to the organ boundary derived from a surface model of the organ and $n_l(\mathbf{x})$ is its l^{th} scalar component, then $u_l^{\perp}(\mathbf{x}) = \left(u(\mathbf{x})^T n(\mathbf{x})\right) n_l(\mathbf{x})$.

The diffusion tensor

$$P(\mathbf{x}) = n(\mathbf{x}) n(\mathbf{x})^T \qquad (2)$$

smooths in the normal direction alone, while the diffusion tensor $I - P(\mathbf{x})$ smooths in the tangential plane. We therefore define the intra-organ smoothness and inter-organ coupling diffusion tensors as:

$$\begin{aligned} D_{IOS}(\mathbf{x}) &= I - w(\mathbf{x}) P(\mathbf{x}) \\ D_{IOC}(\mathbf{x}) &= w(\mathbf{x}) P(\mathbf{x}) \end{aligned} \qquad (3)$$

The weighting term $w(\mathbf{x})$ equals one at organ borders and decreases as a function of the distance $d(\mathbf{x})$ to the organ boundary. $w(\mathbf{x})$ can be formulated as $w(\mathbf{x}) = e^{-\lambda d(\mathbf{x})}$ (exponential decay) or $w(\mathbf{x}) = \frac{1}{1+\lambda\gamma e^{-\lambda d(\mathbf{x})^2}}$ (Dirac function [8, 10]). Within organ interiors, $w(\mathbf{x}) \approx 0$ and the sliding organ regularization tends to the diffusive regularization $S_{diffusive}(u) = \frac{1}{2}\sum_{l=x,y,z}\sum_{\mathbf{x}\in\Omega}\|\nabla u_l(\mathbf{x})\|^2$, which enforces smooth motion in all directions and serves as a point of comparison in this study.

2.4 Geometry conditional deformable image registration

Regions within medical images can be classified into four types: homogeneous regions, and those representing planes, tubes, and small point-like (spherical) structures. We would like to recover sliding motion for both planar and tubular structures. Examples of registrations involving the later include registration of images showing contrast agent flowing through vessels or needles moving through tissue.

In the geometry conditional regularization, we include explicit planar, tubular and point-like structure classifications and aim to recover large and discontinuous deformations. The intra-organ smoothness constraint ensures displacement field smoothness within individual structures and the inter-organ coupling constraint propagates locally detectable displacements to their neighborhood. Discontinuities are allowed to develop where there is tangential movement of planes or tubes. Tube segmentations are stored as centerline+radius+normals measurements and can be extracted using methods such as that described in [1]. Since correspondence for a point-like structure is unambiguous, its displacement vectors should be propagated to its surroundings and the diffusive regularization is appropriate. Forsberg *et al.* [3] also integrate concepts of local structure but do not model sliding motion.

The sliding geometries regularizer is formed by substituting new definitions for $u_l^{\perp}(\mathbf{x})$ and $P(\mathbf{x})$ used in equations (1) and (3). Note that planar, tubular and point-like structures have one, two and three normals, respectively. Based on the local geometry, we include up to three normals at each coordinate, $n_0(\mathbf{x})$, $n_1(\mathbf{x})$, $n_2(\mathbf{x})$, and we add the structure-dependent variables $a_1(\mathbf{x})$ and $a_2(\mathbf{x})$ (planes: $a_1 = a_2 = 0$; tubes $a_1 = 1, a_2 = 0$; points $a_1 = a_2 = 1$). Define $N(\mathbf{x})$ as the 3×3 matrix $[n_0(\mathbf{x}), n_1(\mathbf{x}), n_2(\mathbf{x})]$, A as a 3×3 diagonal matrix whose diagonal elements are (1, $a_1(\mathbf{x})$, $a_2(\mathbf{x})$), and $N_l(\mathbf{x})$ as the column vector of the l^{th} components of the (up to) three normals. The scalar components of the normal displacements $u^{\perp}(\mathbf{x})$ can now be written as:

$$u_l^{\perp}(\mathbf{x}) = \left(N(\mathbf{x})A(\mathbf{x})N_l(\mathbf{x})\right)^T u(\mathbf{x}) \tag{4}$$

Similarly, equation (2) is extended to write the diffusion tensor $P(\mathbf{x})$ that smooths in the normal direction alone as:

$$\begin{aligned} P(\mathbf{x}) &= N(\mathbf{x})A(\mathbf{x})N(\mathbf{x})^T \\ &= n_0(\mathbf{x})n_0(\mathbf{x})^T + a_1(\mathbf{x})n_1(\mathbf{x})n_1(\mathbf{x})^T + a_2(\mathbf{x})n_2(\mathbf{x})n_2(\mathbf{x})^T \end{aligned} \tag{5}$$

This formulation approximates the diffusive regularization at point-like structures, where $a_1(\mathbf{x}) = a_2(\mathbf{x}) = 1$, and within organ interiors, where $w(\mathbf{x})$ approximates zero. Near planar objects, the regularization equals the sliding organ regularization presented earlier.

2.5 Optimization

We use a gradient descent scheme to minimize the cost function $C(u)$ using the regularization defined in equation (1). Without loss of generality, and since we focus on monomodal registration of CT images, we use the sum of squared differences image similarity metric for $D[T, M; u]$. On each registration iteration, the sliding geometries regularization induces an update to the displacement field equal to $-\nabla_u S(u) \triangle t$ at each coordinate $\mathbf{x}$, where $\nabla_u S(u)$ is the gradient of equation (1) with respect to a small perturbation and $\triangle t$ is the time step. Dropping the $(\mathbf{x})$ notation,

$$\begin{aligned} \nabla_u S(u) = -\sum_{l=x,y,z} & \operatorname{div}((I - wP)^T((I - wP)\nabla u_l + wP\nabla u_l^{\perp}))e_l \\ & + \operatorname{div}(wP^T((I - wP)\nabla u_l + wP\nabla u_l^{\perp}))NAN_l \end{aligned} \tag{6}$$

where e_l is the l^{th} canonical unit vector (ex. $e_x = [1, 0, 0]^T$). At convergence, this gradient must be balanced with the gradient from the image similarity measure.

3 Validation

3.1 Inhale/exhale abdominal CT registration

Respiration induces significant and complex deformations to the abdominal organs, including sliding motions between several semi-independent organs. An arterial abdominal CT image acquired at inhale (target) was registered with a hepatic-venous abdominal CT image (moving) from the same patient acquired at exhale (size $240 \times 170 \times 150$; spatial resolution 1.5mm^3). Segmentations of the liver, left and right kidneys, and bones were created semi-automatically in the target image and used to generate surface models defining organ boundaries and normals. Following initial rigid alignment between the two images, the sliding organ deformable registration algorithm described in Section 2.3 was applied in a multi-resolution framework using two resolution levels, the first downsampling by a factor of two and the second operating at native resolution. The registrations took 1000 and 3000 iterations, respectively, with time step 0.046875 s, empirically-determined parameters $\lambda = 0.2$ (for exponential decay) and $\alpha = 24/8$, and were repeated using the diffusive regularization for comparison.

Figure 1 shows the alignment between the target and deformed moving images following sliding organ registration. The alignment was validated quantitatively by segmenting the liver, kidneys and bones in the moving image, warping the resulting label map by the registration displacement field, and calculating

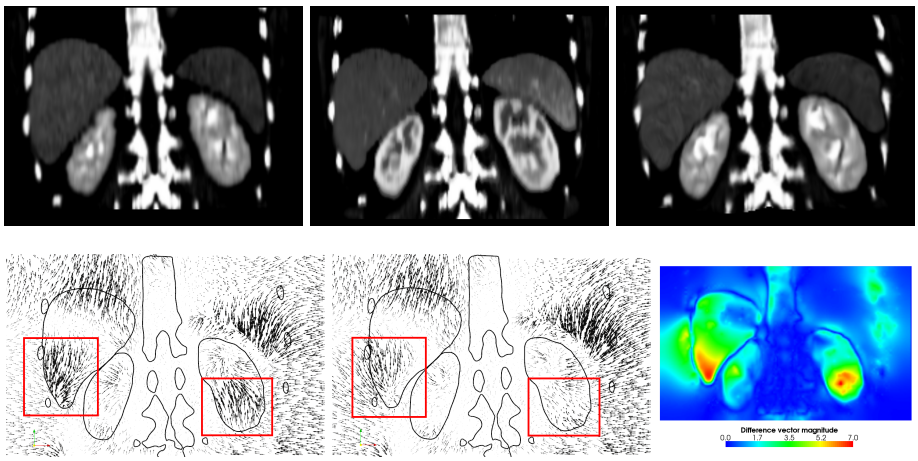

Fig. 1: *Top:* Coronal slice through the (left) moving, (center) target, and (right) transformed moving abdominal CT images using the sliding organ registration. *Bottom:* Coronal slice through the displacement fields from the (left) sliding organ and (center) diffusive registrations, with overlaid anatomical outlines for context, plus (right) the difference vector magnitudes between the displacement fields from the two registrations (best viewed in colour online).

the Dice coefficients between them and segmentations within the target image (Table 1). The results show good overlap between anatomical structures following image registration using the sliding regularization and comparable accuracy to the diffusive regularization.

The improvements of the sliding organ registration lie in the derived correspondences. Figure 1 shows representative coronal slices through the displacement fields from registration with the sliding organ and diffusive regularizations, and the magnitudes of their voxel-wise difference vectors. Unlike the diffusive regularization, the sliding organ regularization preserves the independent and sliding motion of the liver and kidneys. The difference vector magnitude image shows that allowing sliding motion at organ borders causes significant differ-

Table 1: Dice coefficient for organ mask overlap between target images and deformed moving images of registered abdominal images, after registration using the sliding organ and diffusive regularizations.

Organ	Sliding	Diffusive
Liver	0.946	0.945
Right Kidney	0.877	0.870
Left Kidney	0.888	0.896
Bones	0.826	0.840

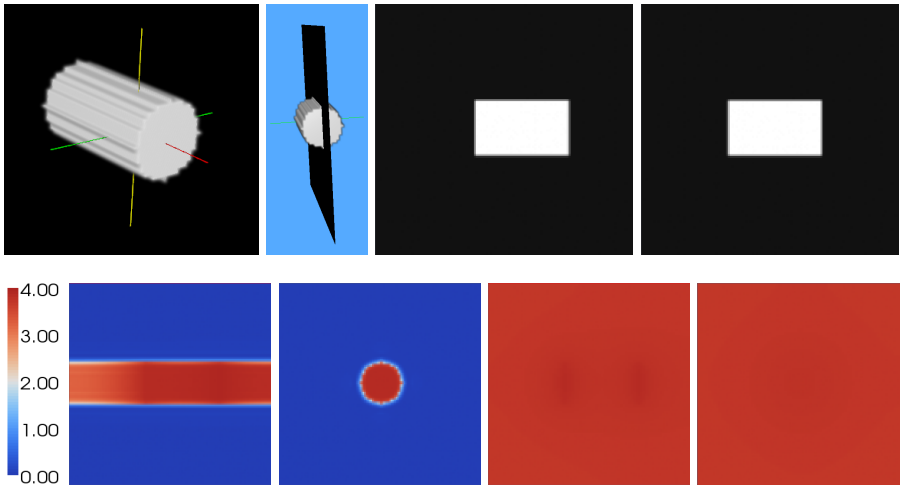

Fig. 2: *Top:* (left) Volume rendering of the sliding tube within the target image, plus slices along the tube's long axis for the (center) target and (right) moving images. *Bottom:* Representative long-axis and cross-sectional slices through the displacement magnitudes resulting from registration with the (left) geometry-conditional and (right) diffusive regularizations (best viewed in colour online).

ences in the motion interpolated deep within organs, leading to greatly altered detected correspondences of up to 7mm.

3.2 Artificial images of a sliding tube

We used the geometry conditional deformable registration algorithm described in Section 2.4 to register artificial images of a tube sliding along its long axis (size $80\times80\times80$; spatial resolution 1mm^3) (Figure 2). Registration was performed using a single resolution level, and compared to the results from the diffusive regularization (8000 and 190000 iterations required to recover the 4mm motion at the tube's edge, respectively, with time step 0.125, λ=0.25, γ=1000, α=1).

As shown in Figure 2, registration with the geometry conditional regularization nicely recovers and constrains the longitudinal motion within the tube. The background material correctly moves with the tube at its two ends, preventing folding, while motion is not interpolated to the stationary background elsewhere. In contrast, registration with the diffusive regularization incorrectly blends the tube's motion within the entire background.

4 Conclusions

In this paper, we have presented sliding organ and geometry conditional regularizations for deformable image registration, to align image pairs exhibiting

large and complex deformations with a focus on handling sliding motion. By taking advantage of local structure information modeled as surfaces and tubular structures, these registration techniques increase the plausibility of the resulting displacement fields while maintaining registration accuracy as measured by image match. In the domain of abdominal imaging, such improved correspondence detection has implications for more accurate image-guided interventions, longitudinal and intersubject analysis, and application of atlas information to individuals. Future work includes additional quantitative validation of correspondence accuracy, application of the geometry conditional regularization to clinical images, and investigations into alternatives to requiring a detailed prior segmentation.

The registration software is available at `http://public.kitware.com/Wiki/TubeTK`. This work was sponsored in part by: (1) NIH/NCI 1R01CA138419-01; (2) NIH/NIBIB 2U54EB005149-06; (3) NIH/NCI 1R41CA153488-01; (4) NSF EECS-0925875; (5) NIH/NIMH 1R01MH091645-01A1; (6) NIH/NIBIB 5P41EB002025-27; (7) NIH/NCI 1R41CA153488-01.

References

1. Aylward, S., Bullitt, E.: Initialization, noise, singularities, and scale in height ridge traversal for tubular object centerline extraction. IEEE Transactions on Medical Imaging 21(2), 61–75 (2002)
2. Cahill, N., Noble, J., Hawkes, D.: A Demons algorithm for image registration with locally adaptive regularization. In: G.Z. Yang et al. (ed.) MICCAI 2010, LNCS, vol. 5761, pp. 574–581. Springer-Verlag, Berlin Heidelberg (2009)
3. Forsberg, D., Andersson, M., Knutsson, H.: Adaptive anisotropic regularization of deformation fields for non-rigid registration using the morphon framework. In: Proc. IEEE ICASSP. pp. 473–476 (2010)
4. Heinrich, M., Jenkinson, M., Brady, M., Schnabel, J.: Discontinuity preserving regularization for variational optical-flow registration using the modified lp norm. In: B. van Ginneken et al. (ed.) Medical Image Analysis for the Clinic - A Grand Challenge, workshop MICCAI 2010, pp. 185–194 (2010)
5. Modersitzki, J.: Numerical methods for image registration. Oxford University Press (2004)
6. Pace, D., Enquobahrie, A., Yang, H., Aylward, S., Niethammer, M.: Deformable image registration of sliding organs using anisotropic diffusive regularization. In: Proc. IEEE ISBI, pp. 407–413 (2011)
7. Ruan, D., Esedoglu, S., Fessler, J.: Discriminative sliding preserving regularization in medical imaging registration. In: Proc. IEEE ISBI. pp. 430–433 (2009)
8. Schmidt-Richberg, A., Ehrhardt, J., Werner, R., Handels, H.: Slipping objects in image registration: Improved motion field estimation with direction-dependent regularization. In: G.Z. Yang et al. (ed.) MICCAI 2009, LNCS, vol. 5761, pp. 755–762. Springer-Verlag, Berlin Heidelberg (2009)
9. Stefanescu, R., Pennec, X., Ayache, N.: Grid powered nonlinear image registration with locally adaptive regularization. Medical Image Analysis 8, 325–342 (2004)
10. Yin, A., Hoffman, E., Lin, C.: Lung lobar slippage assessed with the aid of image registration. In: T. Jiang et al. (ed.) MICCAI 2010, LNCS, vol. 6362, pp. 578–585. Springer-Verlag, Berlin Heidelberg (2010)